XII International Conference on Computational Plasticity. Fundamentals and Applications
COMPLAS XII
E. Oñate, D.R.J. Owen, D. Peric and B. Suárez (Eds)

# RELATIVE CONTRIBUTIONS OF SOLID SKELETON VISCO-PLASTICITY AND WATER VISCOSITY TO THE PORO-MECHANICS BEHAVIOR OF CALLOVO-OXFORDIAN CLAYSTONE

**S. Rahal*, G. Casaux-Ginestet* and A. Sellier***

* Laboratoire Matériaux et Durabilité des Constructions
Université de Toulouse; UPS, INSA; LMDC
135, avenue de Rangueil; F-31 077 Toulouse Cedex 04, France
e-mail: rahal@insa-toulouse.fr - Web page: http://www.lmdc.fr/

**Key words:** Claystone, Viscosity, Time, Creep, Damage

**Abstract.** The Callovo-Oxfordian claystone is a saturated porous medium. Its transfer properties, including its low permeability [16] make it an interesting candidate for underground radioactive waste disposal.
The drained tests performed on the claystone, collected by ANDRA[1] from samples at 500 meters depth [16, 9], exhibits a damageable visco-elasto-plastic behavior. This viscous behavior includes both the viscosity of the skeleton and the water. In existing models [5, 6, 11, 1], the creep phenomena are attributed either to the water permeability, to the skeleton visco-plasticity or sometimes both [13].
In a first step, a simplified analysis is proposed to understand the contribution of each phenomenon with respect to the consolidation time. This study indicates that the apparent characteristic time is the sum of those related to the skeleton and water permeability.
To handle both non-linear and viscous phenomena, the damage law [15], coupled with the basic creep model [14] is used to characterize the solid skeleton of the claystone. The fluid behavior is integrated with the poro-mechanical model [7] implemented in the finite element code CAST3M [4]. The proposed model (visco-elastic damageable skeleton + saturating fluid) is used to simulate an excavation from the ANDRA underground laboratory (located in Bure–France).
This application allows the understanding of how both viscous phenomena combine at each step of the calculation. Just after the excavation, water overpressure decreases near the gallery approaching zero due to the damage and then increases the permeability. The viscosity is then controlled by the solid skeleton creep rates. Later, the redistribution of hydraulic pressure is of more importance and permeability again plays a major role.

[1]The French Agency in charge of the management of radioactive waste disposal.

## 1 INTRODUCTION

Due to their radionuclide retention capacity, high mechanical strength and very low permeability, east argillites are studied as geological barriers for the deep-storage of radioactive wastes disposal. To do so, special attention must be paid to their hydromechanical long-term behavior in order to ensure the required safety conditions for the long-term repository of radioactive waste.

Nowadays, the theory of poro-elasticity is used more frequently for mechanics applications, ranging from civil (rock, concrete, freezing materials...) to petroleum engineering. In this theory, the delayed behavior of the material is induced by the water diffusion processes. In fact, if the skeleton is dry, there is no longer delayed behavior but only instantaneous elastic strain.

By comparing the characteristic time of consolidation predicted by the poro-elastic theory to the experimental results on claystone, [9] exhibits that the delayed effect could not be explained by only pore pressure dissipation, because it includes creep phenomena (it is due to the high clay content[2]). Furthermore, the observed experimental strains are greater than those predicted by the elastic theory [9, 16]. Such strains are essentially related to the inelastic deformations occurring by clay sheet sliding [5].

The existing poro-plastic models [6, 11] are suitable to describe the irreversible strains, however they cannot explain the delayed behavior of the skeleton since it does not affect the apparent characteristic time, driven mainly by the permeability of the material in these models. So, resorting to a poro-visco-plastic formulation could be more realistic.

The first part of this work deals with the understanding of the effect of the skeleton viscosity on the consolidation time. To do so, we propose to compare the characteristic consolidation time of a simplified creep model coupled with or without water. In the second part, the existing creep model [14] is used to characterise the viscous skeleton of the argillaceous formation. The parameters of the model are determined by an inverse analysis through an uniaxial creep test [10]. The proposed model is then coupled with the effective Biot theory [3] in the finite element code CAST3M [4]. The relevance of such modelling is justified by simulating an excavation from the Bure laboratory.

The excavation process creates a perturbed zone around storage structure, where mechanical and hydromechanical properties are altered. The introduction of a damage law is then required in order to reproduce the deterioration of the mechanical features of the material. The orthotropic damage law [15] for brittle materials is chosen to describe the damageable solid skeleton of the stone. Finally, in order to reproduce the deterioration of the hydromechanical properties, we propose to use a law to characterise the increasing evolution of the permeability with respect to the damage.

Pressure fields and convergences of the gallery are compared with experimental measurements [2, 10] over a 2 year period in the tunnel system of the Callovo-Oxfordian formation.

[2]The mineralogy composition contains: quartz (23%), calcite (27%) and clay minerals (45%).

## 2 THEORETICAL PORO-MECHANIC BACKGROUND

This study is carried out in the framework of the theory of poro-elasticity as initially presented by Biot [3] and later elaborated by other authors [7]. The surrounding rock mass is assimilated to a continuous medium (a skeleton and saturating fluid). The compressibility of the skeleton and the fluid, the small strains and transformations, the small variations of porosity and fluid density are assumed. Under these assumptions, the total stress tensor $\boldsymbol{\sigma}$ can be split into an effective part $\boldsymbol{\sigma}'$ applicable on the skeleton and a hydraulic part $-bp\mathbb{1}$ applicable on the saturating fluid. $\boldsymbol{\sigma} = \boldsymbol{\sigma}' - bp\mathbb{1}$.
Where, $p$ denote the pressure of the fluid, $b$ is the Biot coefficient. $b$ is expressed as function of the poro-elastic properties $K_0$ and $K_s$, the drained bulk modulus and the bulk modulus of the skeleton, respectively. $b = 1 - \frac{K_0}{K_s}$.

Let $m_f d\Omega_0$ be the fluid mass contained in the actual volume element $d\Omega_t$. If $\rho_f$ denote the fluid density and $\phi$ the Lagrangian porosity, we have $m_f = \phi\rho_f$. Changes of $\delta m_f$ take into account the variations of volumetric strain $\mathrm{tr}\,\boldsymbol{\varepsilon}$ and pressures $p$: $\delta m_f = \rho_{f_0}\left(b\mathrm{tr}\,\boldsymbol{\varepsilon} + \frac{p}{M}\right)$.
Where, $M$ is the Biot modulus, it is a function of Biot coefficient, the initial porosity $\phi_0$ and the Bulk modulus of the fluid $K_f$: $\frac{1}{M} = \frac{b-\phi_0}{K_s} + \frac{\phi_0}{K_f}$.

The water diffusion is described by Darcy's law which links the water mass flow rate $\underline{\omega}$ to the dynamic viscosity $\eta_f$ and the intrinsic permeability $k'$. The fluid mass balance can be given as: $\frac{\partial m_f}{\partial t} = -\mathrm{div}\,\underline{\omega}$ where, $\underline{\omega} = -\rho_{f_0}\frac{k'}{\eta_f}\,\underline{\mathrm{grad}}\,p$.

## 3 SIMPLIFIED ANALYSIS FOR CONSOLIDATION

To understand the effect of coupling viscosity with poro-mechanical modelling on the consolidation time, we propose the study of the behavior of 3 porous specimens. The first one corresponds to a saturated elastic solid skeleton (classical poro-elasticity). The second is also saturated but with a visco-elastic skeleton (Kelvin-Voigt: a purely viscous damper and purely elastic spring connected in parallel). The last element is similar to the second one but without water. Attention is given to the characteristic consolidation time of the various systems.
The studied system is an uniaxial creep test with classical oedometer boundary conditions. Let $L$ be the length of the specimen. Initially (at $t = 0$) $p_0 = 0$ and $\sigma_0 = 0$. The loading is applied at $t = 0^+$ at very close to $t = 0$. Drainage occurs in the top of the specimen (application load area). The considered mechanical and hydromechanical parameters are summarized in table 1.

**Table 1**: Parameters for the simplified creep analysis

| $E_0$ | $\nu_0$ | $b$ | $M$ | $\eta_f$ | $\sigma$ | $L$ |
|---|---|---|---|---|---|---|
| 4800 MPa | 0,16 | 0,6 | 4900 MPa | $10^{-9}$MPa.s | -15 MPa | 25cm |

The behavior equations are solved using the finite volume method with an implicit integration scheme. Theoretically, it is unconditionally stable and well adapted for diffusion equations. In the parametric study, only the intrinsic permeability is variable. Let $\tau_e$, $\tau_k$ and $\tau_c$ be the characteristic times of the poro-elastic, the Kelvin-Voigt and the coupled poro-elastic Kelvin-Voigt model, respectively. It corresponds to the time matching with 63% of the final consolidation, starting from the undrained response (see the dashed lines in figures 1 and 2).

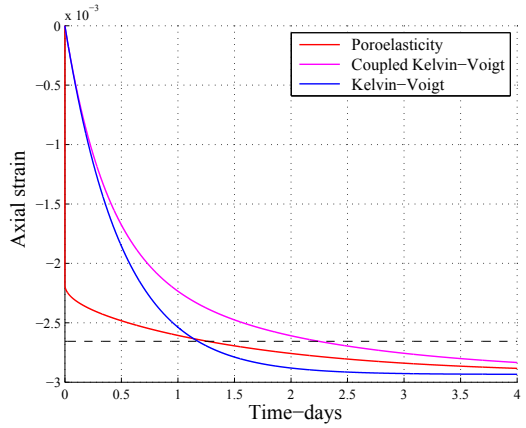


Figure 1: Uniaxial consolidation curves, case $k' = 5.10^{-20}m^2$. $\tau_e = 1,25$, $\tau_k = 1,15$ and $\tau_c = 2,25$ days.

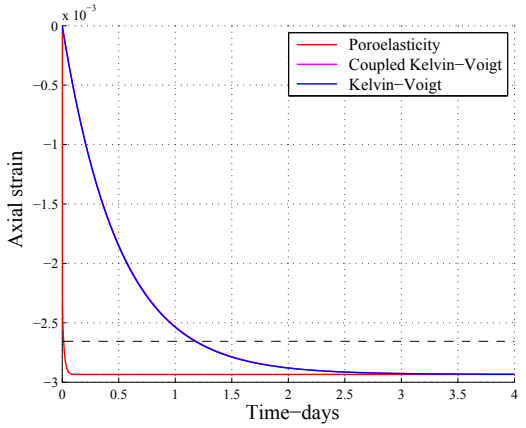


Figure 2: Uniaxial consolidation curves, case $k' = 5.10^{-18}m^2$. $\tau_e = 1,25.10^{-2}$, $\tau_k = 1,15$ and $\tau_c = 1,15$ days.

The results in figure 1 indicate that: if the skeleton is visco-elastic, the characteristic consolidation time is close to the sum of those related to the skeleton and the water ($\tau_c \simeq \tau_k + \tau_e$). Moreover, when $\tau_k \gg \tau_e$ (figure 2), the water diffusion process does no longer effect the consolidation time. The characteristic time is then mostly driven by the consolidation of the skeleton ($\tau_c \simeq \tau_k$).
In real structures, as shown below, both characteristic times evolve due to the non-linear phenomena: permeability increases due to the damage and the visco-plastic characteristic time increases due to the non-linear creep. Consequently, convergence rate of ANDRA's galleries will depend on the evolution of these two characteristic times.

## 4 DESCRIPTION OF THE DAMAGE LAW

A first non-linearity to consider is the argillite damage. Let the stress $\widetilde{\boldsymbol{\sigma}}$ represents the loading effects concentrated in the undamaged zone. This tensor is split into two parts. One for the tension component (positive part of $\widetilde{\boldsymbol{\sigma}}$) the other for the compression one (negative part of $\widetilde{\boldsymbol{\sigma}}$). It allows to compute the tension and the compression damage tensors, $\mathbb{D}^t$ and $\mathbb{D}^c$, respectively, according to the criteria and damage evolution laws described in [15].

The damage in compression is isotropic. It is driven by the Drucker-Prager yield criterion. It corresponds to a diffuse micro-cracking in the material (figure 3). In tension, the damage is orthotropic. It is inspired by the homogenisation theory before the pic phase and driven by the Rankine yield criterion. It corresponds to oriented micro-cracking perpendicular to the main tensile stress (before the pic phase) and localized macro-cracking during the softening phase (after the pic phase).

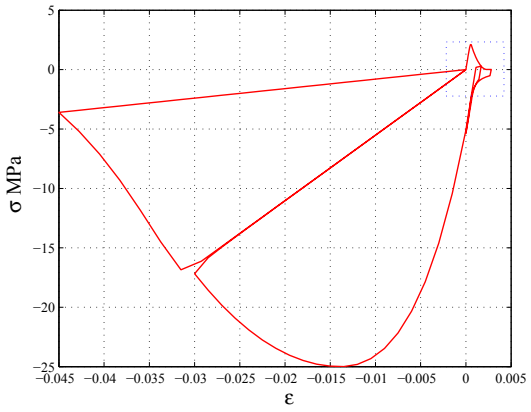


Figure 3: Response of the model for a compression uniaxial cyclic test.

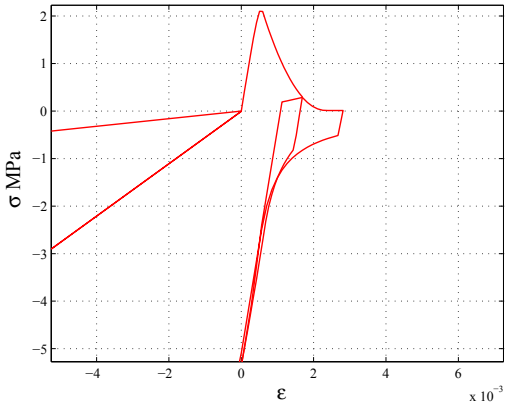


Figure 4: Response of the model for a tension uniaxial cyclic test.

Numerical localization is a specific phenomenon for laws with softening behavior in the finite element software, which is linked to the meshing definition. This phenomenon is due to an ill-posed boundary problem related to a loss of ellipticity of the tangent matrix in the numerical system to be solved. To solve this problem, a crack opening displacement is modelled and embedded in the local form of the constitutive law.
The originality of this model is the progressive hardening of the material in compression after tensional loading is applied (see figure 4). This occurs without any change to the damage tensor, which allows to respect the thermodynamic framework.
The constitutive law is:

$$\boldsymbol{\sigma}' = \left(\mathbb{I} - \mathbb{D}^c\right)\left(\mathbb{I} - \mathbb{D}^t\right)\overbrace{\mathbb{C}^0 : \boldsymbol{\varepsilon}^e}^{\tilde{\boldsymbol{\sigma}}} + \left(\mathbb{I} - \mathbb{D}^c\right)\mathbb{D}^t\overbrace{\mathbb{C}^0 : \left(\boldsymbol{\varepsilon} - \boldsymbol{\varepsilon}^f\right)}^{\tilde{\boldsymbol{\sigma}}^f} \tag{1}$$

Where, $\mathbb{C}^0$ is the stiffness tensor of the undamaged material, $\boldsymbol{\sigma}^f$ is the reclosure stress in a tensile crack, $\boldsymbol{\varepsilon}^e$ is the elastic strain tensor and $\boldsymbol{\varepsilon}^f$ the inelastic strain tensor, it corresponds to the inelastic displacement used to manage the crack reclosure as described in [15].

# 5 RHEOLOGICAL CREEP MODEL FOR CLAYSTONE

## 5.1 Description of the model

The existing creep tests [9, 16, 10] on claystone indicate that:

- Creep occurs even under very low stress level (1,5 MPa),
- Important irreversible strains are observed,
- The creep velocity is continuously decreasing without any lower creep limit,
- Creep occurs by clay sheet sliding.

The rheologic scheme to assess $\widetilde{\boldsymbol{\sigma}}$ allows for the description of most of the observed phenomena. It contains three terms in series. The first one is an elastic level to simulate instantaneous elastic response (subscript e in figure 5.1), the second is a visco-elastic level to simulate reversible delayed strains (subscript KV for Kelvin-Voigt) and a non-linear viscous level (subscript M for Maxwell) to describe irreversible strains [14]. This scheme is applied separately to each component of the $\widetilde{\boldsymbol{\sigma}}$ tensor (spherical 's' and deviatoric 'd' parts).

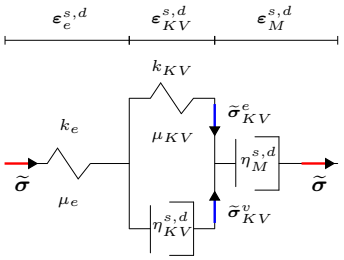


**Figure 5**: Rheological model for claystone.

The partition into spherical and deviatoric parts was initially proposed to describe C-S-H sheet sliding for concrete. It can easily transposed for claystone to describe the sliding of the thin clay layer. Furthermore, the proposed non-linear Maxwell level lets us describe an increasing apparent viscosity $\eta_M$ with respect to the consolidation of the system $C_c$.

$$\eta_M = \eta_{M_0} C_c \qquad \text{with,} \qquad C_c = \exp\left(\frac{\varepsilon^{eq}}{\varepsilon^k}\right) \tag{2}$$

An exponential function for $C_c$ ensures a continuously decreased velocity without any lower creep limit. Where, $\varepsilon^{eq}$ is the equivalent creep strain, it is chosen proportional to the square root of the viscous dissipation. $\varepsilon^k$ is a parameter of the model. It plays the role of a creep strain potential to describe interlocking of the viscous phase (clay) by non viscous inclusions (quartz, calcite ...etc.) as explained in [14].

## 5.2 Determination of the parameters for claystone

The material parameters of the solid skeleton are deduced from a drained uniaxial creep test [10]. The initial Young's modulus and Poisson's ratio of the sample are 4800 MPa and 0,16, respectively. The corresponding curve is presented in figure 6.

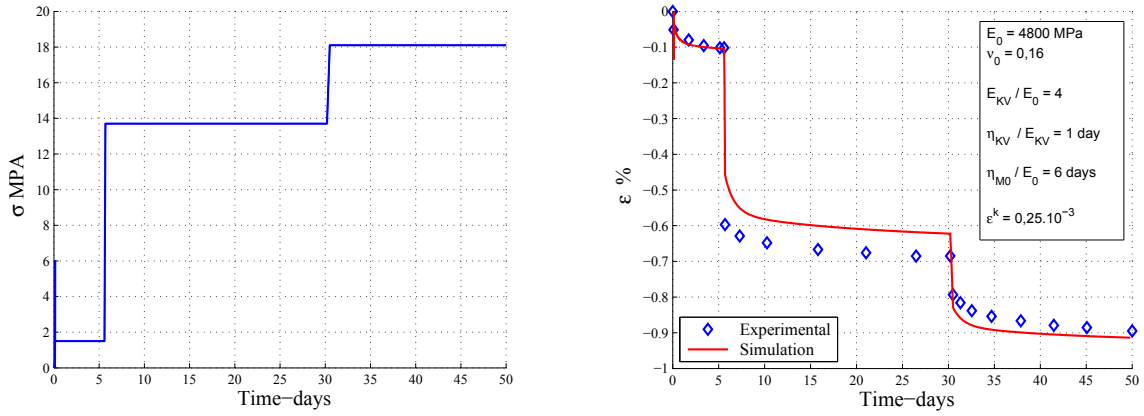


**Figure 6**: Comparison between measurement and the predicted deformation under uniaxial loading.

## 6 NUMERICAL MODELLING OF AN EXCAVATION

### 6.1 Description of the problem

The numerical simulations carried out within the context of this study have been made using a FEM code called CAST3M [4], where the described damage law and the creep model are implemented in the framework of poro-mechanic formulation.
Under these assumptions, the total stress tensor can be expressed as:

$$\boldsymbol{\sigma} = (\mathbb{I} - \mathbb{D}^c)\left\{\left(\mathbb{I} - \mathbb{D}^t\right)\mathbb{C}^0 : (\boldsymbol{\varepsilon} - \boldsymbol{\varepsilon}^{cr}) + \mathbb{D}^t\mathbb{C}^0 : \left(\boldsymbol{\varepsilon} - \boldsymbol{\varepsilon}^f\right)\right\} - bp\mathbb{1} \tag{3}$$

Where, $\boldsymbol{\varepsilon}^{cr}$ is the strain creep tensor.
The numerical modelling is carried out in 2D with plane strain assumptions. Despite this simplified analysis, the out of plane stress is considered as an initial imposed stress and then taken into account in the Drucker-Prager criterion. The symmetry of the problem allows to consider only a quarter of the excavation for modelling.
Another feature of the rock is the anisotropic stress field, which according to [10] is close to $\sigma_v = 12,7$ MPa, $\sigma_h = 12,4$ MPa, $\sigma_H = 14,5$ MPa and a water pressure of 4,9 MPa at 500m depth. That stress state is injected in the initial conditions for calculating the gallery. It is assumed an excavation conducted following the major stress $\sigma_H$.
In order to properly reproduce the deconfinement, the hydomechanical boundary conditions around the wall of the excavation are linearly decreased to zero during 1 day.
The area under investigation and the boundary conditions are summarised in figure 7.
To describe the damageable behavior of the stone, the parameters in table 2 are considered for the damage law. The creep parameters are those determined in figure 6, whereas the hydromechanic parameters ($b$, $M$, $\eta_f$) are those used in the parametric study (see table 1), according to [10].

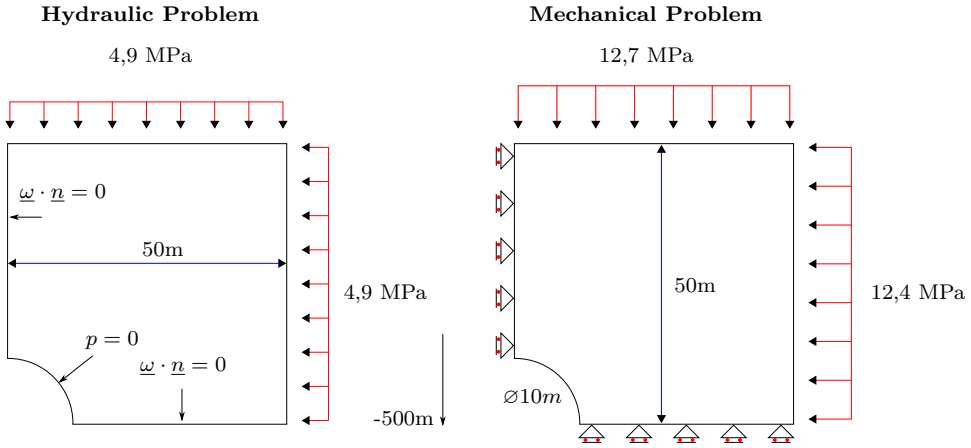


**Figure 7**: Boundary conditions for the coupled hydromechanical problem after excavation is complete.

**Table 2**: Parameters for the damage law [15] to describe the damageable skeleton of claystone.

| **Parameters** | **Value** | **Unit** |
|---|---|---|
| Tensile strength | 2,7 | MPa |
| Fracture Energy in tension | $10^{-4}$ | M.N/m |
| Compressive strength | 25 | MPa |
| Fracture Energy in compression | $3,5.10^{-2}$ | M.N/m |
| Characteristic width of a crack | 30 | $\mu m$ |
| Friction angle in a crack | 19 | degrees |
| Crack reclosure stress | 5,5 | MPa |

## 6.2 Damageable permeability

During the excavation, the permeability is roughly altered due to the crack openings. According to experimental measurements, permeability increases by a factor greater than $10^4$ in the damaged zone. To our knowledge, there is no significant study at the present days on the evolution of the claystone permeability with respect to the damage. As a first approximation, the following law inspired by existing exponential laws for concrete [12] is proposed:

$$k' = k'_0 \exp\left(\ln\left(\frac{k'_{\max}}{k'_0}\right) D^M\right) \qquad \text{where,} \qquad D^M = 1 - (1 - D^c)(1 - D^t_I) \tag{4}$$

$D^t_I$ is the induced damage in tension in the first main direction and $D^c$ the isotropic damage in compression. Although the damage law is anisotropic, this first approximation considers an isotropic damage permeability. According to [10] the intrinsic permeability of the undamaged stone is close to $k'_0 = 5.10^{-20} m^2$. In this study $k'_{\max} = 10^4 k'_0$.

## 6.3 Results

### 6.3.1 Evolution of Pressure fields

To demonstrate the relevance of such modelling on the long term behavior of the Callovo-Oxfordian claystone, the numerical results are compared with experimental data. [10] provides experimental measures of stabilized pressure fields around different galleries. The experimental points in figure 8 and 9 clearly show a pressure drop in the first 5 meters near the gallery. In fact, without taking into account the increasing permeability with respect to the damage, it is quite impossible to reproduce the observed experimental data (see figure 8). It can be noticed that the dropped pressure zone matches with the damage area (see figure 10).

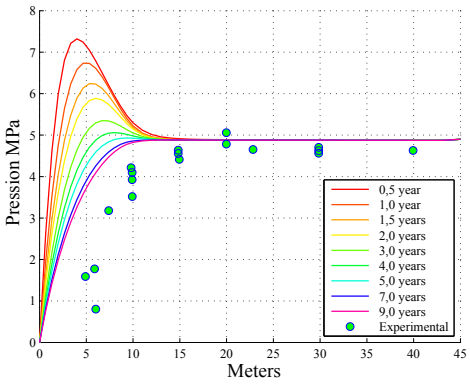


Figure 8: Evolution of pressures at different dates, starting from the gallery walls along the horizontal axis at 500m depth, without changing the permeability.

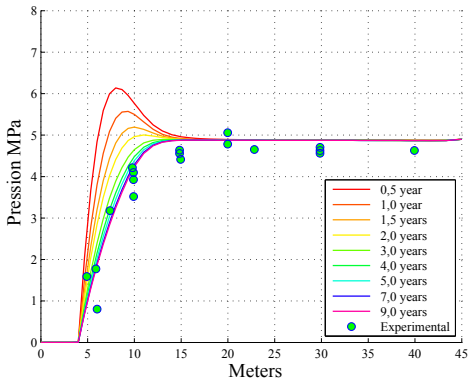


Figure 9: Evolution of pressures at different dates, starting from the gallery walls along the horizontal axis at 500m depth, with a damageable permeability.

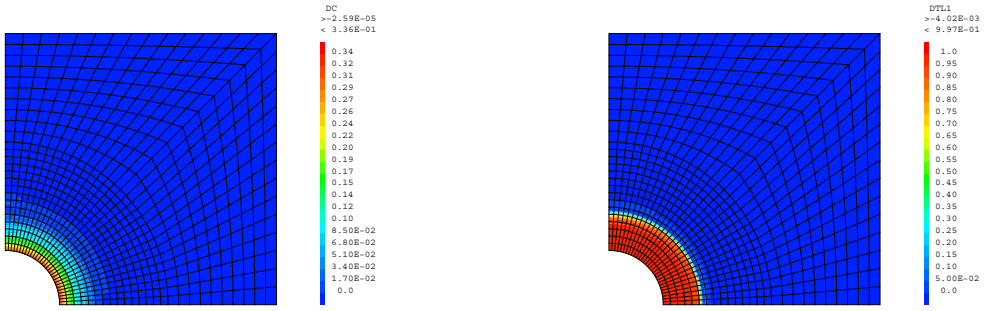


**Figure 10**: Damage fields around the gallery 1 year following the excavation ($D^c$ and $D^t_I$).

### 6.3.2 Convergence of the gallery

Thanks to the experimental results in [8] (measuring device with laser pointer), it is possible to compare the predicted convergence of the gallery walls with experimental results provided by the proposed coupled model. However, there is uncertainty about the exact date of acquisition beginning after the excavation (a few days approximation). In the presented curves, it assumes the displacements are measured 5 days after the beginning of the excavation, that means, the instantaneous displacements during excavation are not considered to compare with experimental results (figures 11 and 12).
On the other hand, this instantaneous convergence is not of great interest to design of concrete vaults which are cast a few days after the excavation. Therefore, it is important to model the convergence from the casting date until a long time period. The convergences of the gallery are plotted and compared with two experimental device results.
In the numerical simulations, 3 cases are considered, poro-mechanic with viscous damageable skeleton, poro-mechanic with viscous skeleton and poro-mechanic with damageable skeleton, respectively. The last case clearly exhibits that the loss of stiffness due to damage coupled with the poro-mechanic theory, cannot explain by itself the observed experimental convergence (the convergence is close to 0,2 mm, 4 years after the beginning the excavation). In fact, the observed experimental strains are mainly induced by the creep of the skeleton (as shown in case 2).

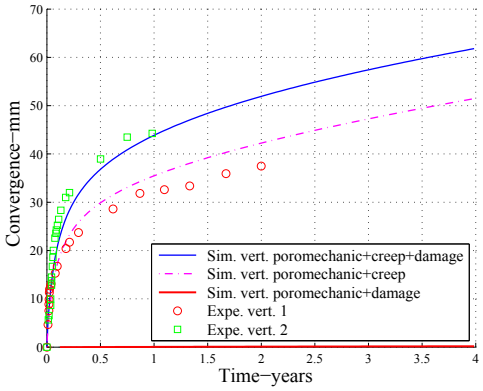


Figure 11: Experimental and numerical vertical convergences of the gallery.

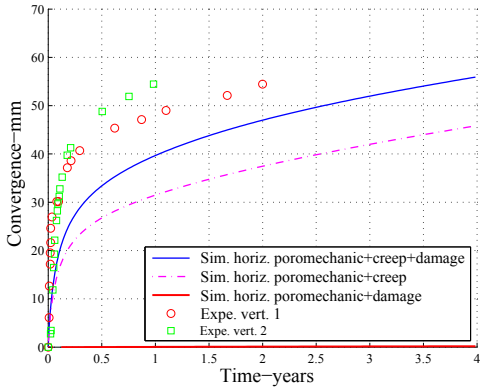


Figure 12: Experimental and numerical Horizontal convergences of the gallery.

By taking into account all the phenomena (poro-mechanic+creep+damage), the comparison between experimental convergence data and the numerical results has shown good agreement. For instance, the vertical convergence matches with the measurement 2 (see figure 11). However, it does not match as well with the corresponding horizontal measurements (see figure 12). In fact, there is some initial anisotropy of the rock which is not taken into account in the proposed model. This could explain the difference between

the vertical and horizontal convergences (since the stress anisotropy is not quite different in both horizontal and vertical directions). In spite of this, the shape of the curve is well respected (convergence velocity) whatever the direction.
Finely, referring to the previous parametric study, the increasing permeability has led to a drop of pressure fields in the damage zone. In this zone, the delayed behavior of the argillites is mostly driven by the creep behavior. In fact, the non-linear Maxwell dumper is well representative of the long term behavior of the Calovo-Oxfordian claystone.

## 7 Conclusion

This work has been devoted to the numerical investigation of the damageable viscous behavior of the Callovo-Oxfordian claystone.

The parametric study has shown the necessity of coupling viscous behavior with Biot theory, leading to the cumulation of their characteristic times.

Experimental observations allowed to select and justify a creep model to describe the viscous behavior of the solid skeleton. For modelling an excavation, an orthotropic damage law is used. Both creep and damage models are coupled with the effective Biot theory. In this modeling, the relationship between the damage and the permeability is considered. Despite the uncertainty of the law for claystone, it reveals that it is necessary to take into account the induced damage of hydromechanical properties.

The proposed model integrates the deformations measured in the laboratory and verifies that they allow to explain those observed in-situ.

In fact, it would be more realistic to integrate a permeability depending not only on the damage but also on the crack openings (since they are already held by the model). For instance, the compression strains can close the existing cracks leading to a decreasing permeability, on the other hand the damage cannot decrease (to ensure the thermodynamic framework). So, resorting to a Poiseuille based law could be a suitable approach to describe the water flow in the crack. Finally, to reflect more accurately the orthotropic damage law, the permeability should be oriented along the localized damage directions. These observations are part of the upcoming improvements.

## REFERENCES

[1] A. Abou-Chakra Guéry, F. Comery, K. Su, J. F. Shao, and D. Kondo. A micromechanical model for the elasto-viscoplastic and damage behavior of a cohesive geomaterial. *Physics and Chemistry of the Earth*, 33:416–421, 2008.

[2] G. Armand. Excavation Damaged Zone (EDZ) : Caractrisation initiale, évolution et impact sur les déformations Centre de Meuse / Haute-Marne. Technical report, ANDRA, 2009.

[3] M. A. Biot. General theory of three dimensional consolidation. *Journal of Applied Physics*, 12(2):155–164, 1941.

[4] CAST3M-2012. http://www-cast3m.cea.fr/.

[5] A. S. Chiarelli, J. F. Shao, and N. Hoteit. Modeling of elastoplastic damage behavior of a claystone. *Int. J. Plasticity*, 19:23–45, 2003.

[6] N. Conil, I. Djeran-Maigre, R. Cabrillac, and K. Su. Poroplastic damage model for claystones. *Applied Clay Science*, 26:473–487, 2004.

[7] O. Coussy. *Mechanics of Porous Continua. English (translation) by F. Ulm.* John Wiley & Sons; 2 Rev Ed edition, November 1995.

[8] R. De La Vaissiere. Expérimentation CDZ. Installation et premier cycle de chargement. Premiers résultats : Centre de Meuse / Haute-Marne. Technical report, ANDRA, 2012.

[9] M. Gasc-Barbier, S. Chanchole, and P. Bérest. Creep behavior of bure clayey rock. *Applied Clay Science*, 26:449–458, 2004.

[10] B. Gatmiri. Synthèse générale du programme 2007-2011 du groupement de laboratoire géomécanique. Technical report, ANDRA, 2011.

[11] D. Hoxha, A. Giraud, F. Homand, and C. Auvray. Saturated and unsaturated behaviour modelling of Meuse-Haute/Marne argilite. *Int. J. Plasticity*, 23:733–766, 2007.

[12] V. Picandet, A. Khelidj, and G. Bastian. Effect of axial compressive damage on gas permeability of ordinary and high-performance concrete. *Cement and Concrete Research*, 31:1525–1532, 2001.

[13] R. Plassart, R. Fernandes, A. Giraud, D. Hoxha, and F. Laigle. Hydromechanical modelling of an excavation in an underground research laboratory with an elastoviscoplastic behaviour law and regularization by second gradient of dilation. *International Journal of Rock Mechanics & Mining Sciences*, 58:23–33, 2013.

[14] A. Sellier, L. Buffo-Lacarrière, S. Multon, T. Vidal, and X. Bourbon. Nonlinear basic creep and drying creep modelling. In *SSCS*, Aix-en-Provence, France, May 29-June 1 2012.

[15] A. Sellier, G. Casaux-Ginestet, L. Buffo-Lacarrière, and X. Bourbon. Orthotropic damage coupled with localized crack reclosure processing. Part I: Constitutive laws. *Engineering Fracture Mechanics*, 97:148–167, 2013.

[16] C. Zhang and T. Rothfuchs. Experimental study of the hydro-mechanical behaviour of the Callovo-Oxfodian argillite. *Applied Clay Science*, 26:325–336, 2004.